Journal of Power Sources 244 (2013) 410–416

Contents lists available at SciVerse ScienceDirect

Journal of Power Sources

journal homepage: www.elsevier.com/locate/jpowsour

Atomic layer deposition of TiO_2 on negative electrode for lithium ion batteries

Meng-Lun Lee [a], Chung-Yi Su [a], Yu-Hung Lin [a], Shih-Chieh Liao [b], Jin-Ming Chen [b], Tsong-Pyng Perng [a], Jien-Wei Yeh [a,*], Han C. Shih [a,c,**]

[a] Department of Materials Science and Engineering, National Tsing Hua University, 101, Section 2, Kuang-Fu Road, Hsinchu 30013, Taiwan
[b] Materials and Chemical Engineering, Industrial Technology Research Institute, 195, Section 4, Chung-Hsing Road, Chutung 31040, Taiwan
[c] Institute of Nanomaterials, Chinese Culture University, 55, Hwa-Kang Road, Yang-Ming-Shan, Taipei 11114, Taiwan

HIGHLIGHTS

- Atomic layer deposition is an effective process to fabricate TiO_2 nano-layer.
- The high uniformity TiO_2-deposited electrode is applied in lithium ion battery.
- TiO_2 deposited electrode enhances the electrochemical performance of Li-ion cells.
- Electrode with TiO_2 shows smaller resistance than controlled one after cell cycling.
- The resistance suppression results in a good cycle stability of the Li-ion cell.

ARTICLE INFO

Article history:
Received 21 September 2012
Received in revised form
28 November 2012
Accepted 1 December 2012
Available online 10 December 2012

Keywords:
Atomic layer deposition (ALD)
Lithium ion battery
Anode
Graphite

ABSTRACT

Atomic layer deposition (ALD) technology consisting of periodically repeated series of self-limited surface reactions is a CVD technique for the well-controlled deposition of inorganic layers with thickness in the nanometer scale which has been widely used in the semiconductor industry. In this study, a novel process to fabricate TiO_2 nano-layer with high uniformity by ALD on the graphite negative electrode of lithium battery is reported. We found that under accurate thickness control, a TiO_2 plated graphite electrode shows better performance in cycle life, compared with the pristine graphite. Electrochemical impedance spectroscopy (EIS) results showed that after 60 cycles, the cell resistance of the TiO_2 plated electrode decreased, while that of normal graphite electrode increased significantly. The enhanced performance of the electrode may be attributed to the TiO_2 plating, which suppressed the increase of resistance during the prolonged cycle.

1. Introduction

Rechargeable lithium ion batteries have been extensively adopted in consumer electronic devices due to their significant advantages such as specific energy and energy density. In the past two decades, carbonaceous materials are widely employed as anode in commercial lithium ion batteries because of their high capacity, stable voltage profile and reasonable cost [1]. Various kinds of carbon such as carbon black, graphite have been used as active material of negative electrode (anode) for lithium-ion batteries [2]. Many researchers have been investigating the improvement of the reversible performance of the carbonaceous materials. Although structural change of these materials plays an important role during the lithium intercalation–deintercalation process, research in recent years has demonstrated that either in the liquid or gelled polymer electrolyte, a passivating layer generally addressed as a solid electrolyte interphase (SEI) is formed on the graphite anode during the first charge [3–6]. Two conventional models include one in which the SEI layer is formed through the co-intercalation of solvent molecules from a decomposed electrolyte, along with lithium ions, then diffused into the graphite anode [7]. The other model is where the SEI is formed by the decomposition of electrolytes on the graphite surface [8]. Since the surface status of

* Corresponding author. Tel.: +886 3 5715131x33868.
** Corresponding author. Department of Materials Science and Engineering, National Tsing Hua University, 101, Section 2, Kuang-Fu Road, Hsinchu 30013, Taiwan. Tel.: +886 3 5715131x33845; fax: +886 3 5710290.
E-mail addresses: jwyeh@mx.nthu.edu.tw (J.-W. Yeh), hcshih@mx.nthu.edu.tw (H.C. Shih).

0378-7753/$ – see front matter © 2012 Elsevier B.V. All rights reserved.
http://dx.doi.org/10.1016/j.jpowsour.2012.12.005

anode during electrochemical reaction in a lithium-ion battery is indeed a very complicated phenomenon, there is no absolute conclusion regarding the detailed mechanism up to now. The SEI formation is not only associated with the irreversible charge loss but does also affect the long term cycling stability of the lithium-ion cells. It is believed that the parameters and the characteristics of the SEI film could be the most critical factors affecting the performance of carbon electrodes [9–14]. In an ideal case, the roles which could be expected from SEI are physically/electronically isolating the electrolyte from electrode to stop the further electrolyte decomposition and permitting the transportation of lithium ions to guarantee the ion conductivity [15]. An effective and stable SEI would result in good electrochemical properties during the prolonged cycling of the Li-ion cell [16]. However, the fabrication of SEI significantly depends on the electrode surface accessible to the electrolyte. Besides the composition of the electrolyte, the formation of SEI mainly determined by the electrode morphology, including surface area, particle size, shape, porosity, etc. [17].

Research on the surface phenomena of graphite anodes focuses mainly on the modification of the graphite surface which could be an effective approach to improve its electrochemical performance [11,17–24]. Guo et al. improved cycling performance of natural graphite by coating poly-acrylonitrile on the surface of graphite particles via radiation-initiated polymerization [18]. Zhao et al. modified the graphite by a carbon-film encapsulation and reduced its BET surface area in order to minimize the irreversible capacity by reducing the formation of SEI film during the first intercalation process [19]. Other researchers improved rate capability and cycling stability of cells by coating the carbon anode with metal oxides such as Al_2O_3, $Li_4Ti_5O_{12}$ or TiO_2 [20–24] to decrease the interfacial resistance on the electrode/electrolyte interface. Zhang et al. also reported that core-shell structured electrode materials could improve cycling behavior [23]. However, the synthesis of these composites with well-controllable phase and structure generally pass through a rather complicated procedure and consequently retail at a very high cost.

Atomic layer deposition technology consisting of periodically repeated series of self-limited surface reactions is a CVD technique for the well-controlled deposition of the inorganic layers with thickness in the nanometer scale. It has been widely used in the semiconductor industry to induce the growth of high-k dielectric films of the metal oxide–semiconductor field-effect transistors [25–27]. In addition, the self-limiting gas–solid growth characteristics of the ALD facilitate the growth of thin films or nanoparticles with accurate thickness control and good uniformity [28]. Recent researches have demonstrated that the ALD technique can not only synthesize new components for high-performance lithium ion batteries, including anodes, cathodes, and solid state electrolytes, but also modify the characteristic of electrodes via surface coating [29]. Consequently, ALD could be considered as an efficient route for the surface modification on the graphite negative electrode for lithium ion battery applications.

In this research, a novel process to fabricate TiO_2 nano-layer with high uniformity by ALD on the graphite negative electrode of lithium battery is reported. The TiO_2 polymorphs are recently regarded as an ideal anode material with its long cycling stability due to small volume change during the lithium insertion and extraction process [30]. In addition, the high voltage plateau of TiO_2 (i.e., 1.5–1.8 V vs. Li^+/Li) minimizes formation of the SEI on its surface. In the present study, the morphology and the composition of the electrode surface were investigated by SEM and XPS, respectively. The electrochemical properties of the prepared negative electrode (anode) were studied and the underlying mechanism will also be discussed.

2. Experimental

2.1. Preparation of electrodes

Before depositing TiO_2 nanoparticles on the graphite negative electrode, a water-based slurry consisting of 90 wt.% of graphite powder (Spherical/$D_{50} = 12$ μm, BTR, Shenzhen), 8 wt.% of aqueous polyacrylic latex binder (LA132, INDIGO, Chengdu), and 2 wt.% of conductive carbon (KS4, TIMCAL) was coated onto the Cu foil (NIPPON FOIL) by the comma coater (HIRANO TECSEED, TM-MC) to provide a typical electrode as a substrate. The electrode was then vacuum-dried overnight at 90 °C. TiO_2 nanoparticles were deposited onto the electrode surface by 0–400 ALD reaction cycles consisting of alternating exposure to $TiCl_4$ (Aldrich) and H_2O (99.999%) at room temperature. The reactions were done by a home-made cross-flow ALD system with the diameter of 6 in. During ALD, the reactor was under a constant pressure of 1.0 Torr. In each cycle, an 80 ms $TiCl_4$ pulse and an 80 ms H_2O pulse were separated by 5 s of purging with N_2 (99.9995%). The morphology and chemical composition of the electrode were examined using a field-emission scanning electron microscope (JEOL, Tokyo, Japan, JSM-6500F), and X-ray photoelectron spectroscopy (XPS, Perkin–Elmer, Norwalk, CT, PHI1600).

2.2. Electrochemical measurements

Galvanostatic charge–discharge measurements of the working electrodes were carried out using coin-type cells. The lithium metal (Chemetall Foote Corp., NC, USA) was used as a counter electrode in the cell. The 2032 coin cells were assembled using the copper foil as an anode in an argon glove box where both moisture and oxygen contents were <2 ppm. The mass of the electrodes was 17–19 mg cm^{-2}. The electrolyte was composed of 1 M $LiPF_6$ in a 3:1:4:2 (volume ratio) mixture of ethylene carbonate (EC)/propylene carbonate (PC)/ethyl methyl carbonate (EMC)/dimethyl carbonate (DMC) (SAMSUNG). The electrochemical properties of the cell were tested with the multi-channel automatic battery cycler (Arbin) at a constant charging current from 0.05 C to 6 C. The cut-off voltages were set at 1.5 V and 0.01 V.

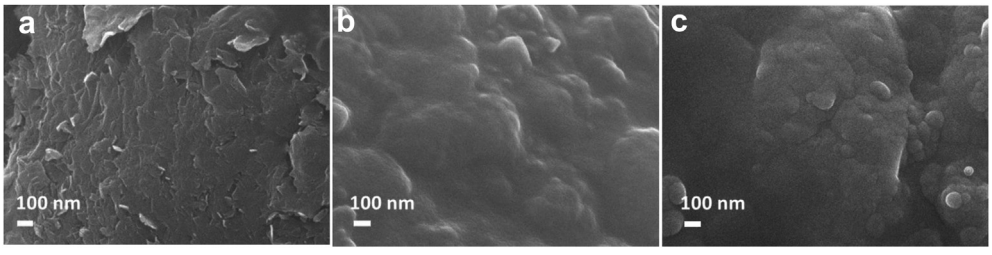

Fig. 1. SEM images of (a) pristine graphite electrode, the graphite electrodes obtained after (b) 200 and (c) 400 ALD reaction cycles.

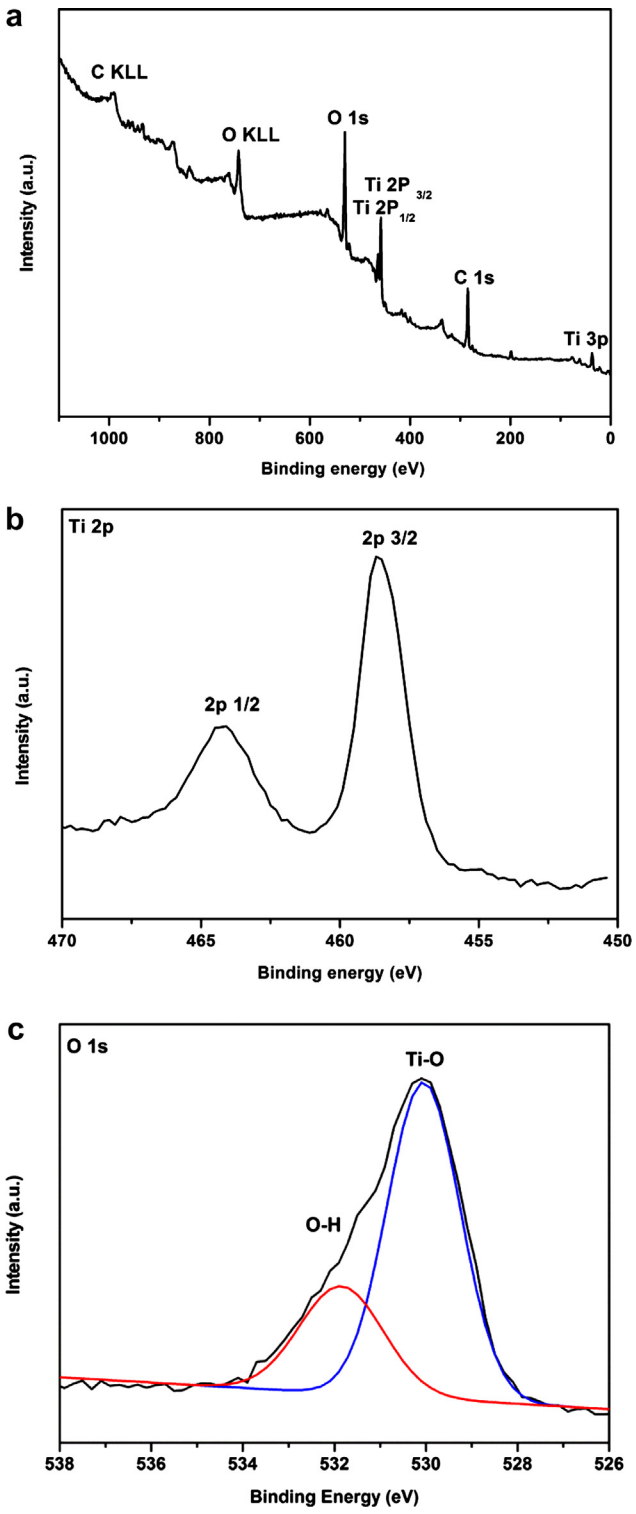

Fig. 2. XPS spectra of the TiO_2-deposited graphite electrode: (a) survey scan, (b) Ti 2p, and (c) O 1s core-level spectrum.

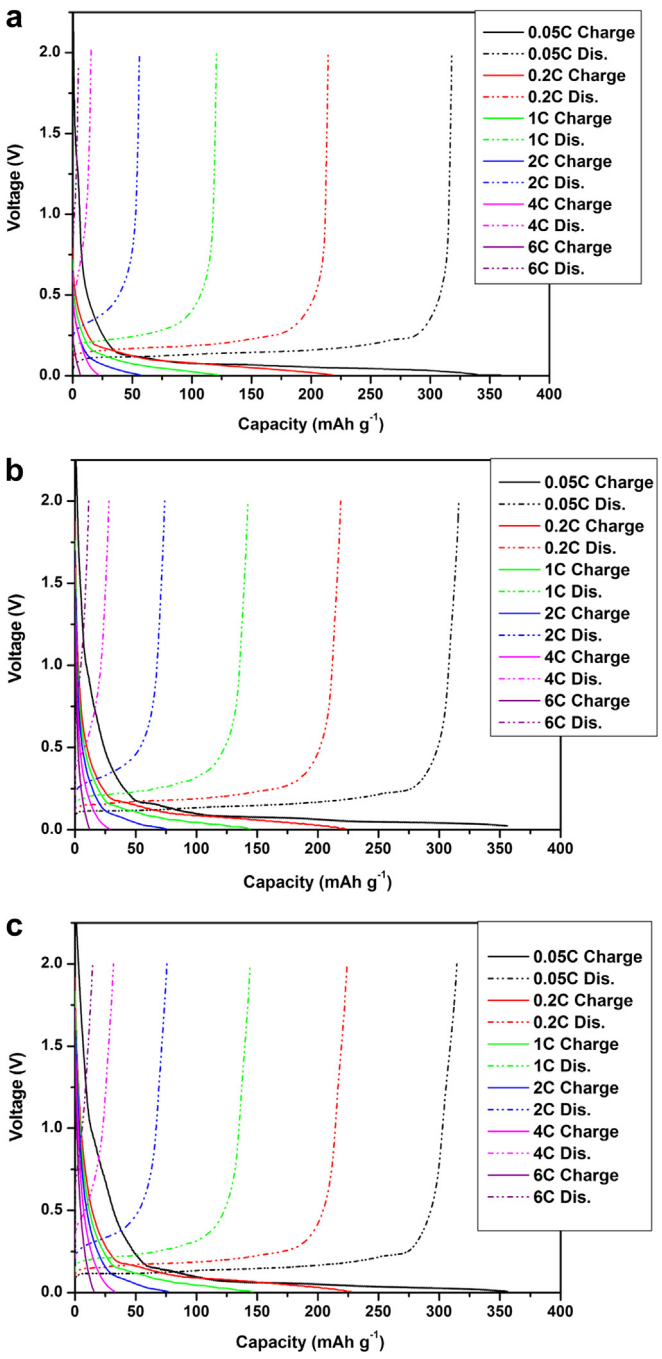

Fig. 3. Galvanostatic charge (lithium intercalation)–discharge (de-intercalation) curves of the (a) pristine graphite electrode, TiO_2-deposited graphite electrode obtained by (b) 200 ALD reaction cycles and (c) 400 ALD reaction cycles.

Electrochemical impedance spectroscopy (EIS) has been widely used in the analysis of electrochemical intercalations of Li ions into carbonaceous materials and transition metal oxides. Lithium insertion involves a series of complex phenomena including lithium ion diffusion in the electrolyte, migration through the SEI film covered on the electrode, charge transfer between the electrode and the electrolyte, the solid state diffusion in the material bulk, etc. [24,31,32]. In this research, EIS measurements of the cells were conducted using an electrochemical measurement unit (Solartron Instruments, SI1280B). The frequency range and voltage amplitude were set from 100 kHz to 0.01 Hz and at 5 mV, respectively. The Code ZView software was used to fit the spectra to the possible equivalent circuit.

3. Results and discussion

3.1. Component and morphology of the materials

Fig. 1 illustrates the morphology of the pristine graphite electrode and the final products obtained after 200 and 400 ALD

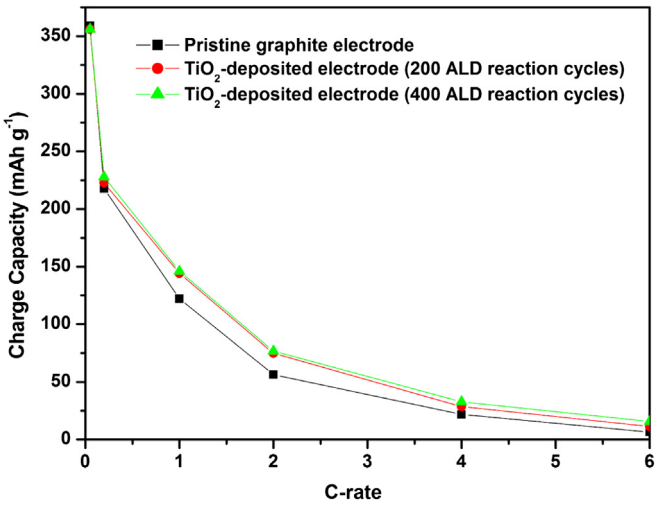

Fig. 4. Charge (lithium intercalation) capacity of the pristine graphite electrode and the TiO_2-deposited graphite electrodes at various C-rates.

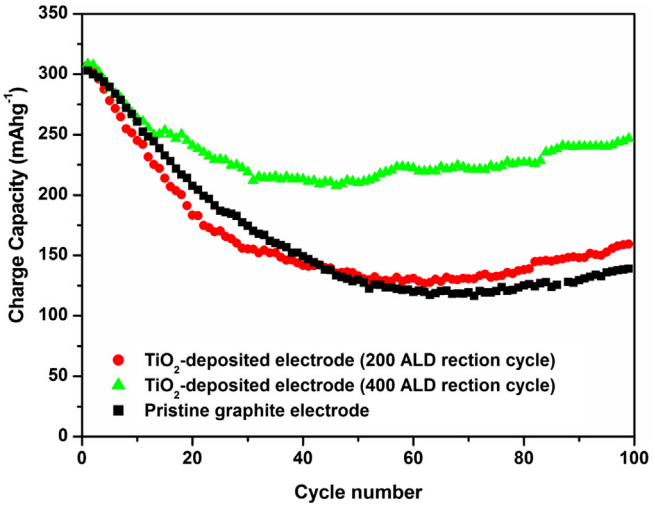

Fig. 5. Cycle life testing of the graphite electrode and the TiO_2-deposited graphite electrodes following the constant charge (lithium intercalation)–discharge (de-intercalation) rate of 0.2–0.5 C.

reaction cycles, respectively. It is seen that the surface of original electrode is rather rough, as shown in Fig. 1(a). In Fig. 1(b) and (c), the results revealed that many nanoparticles were uniformly dispersed on the electrode to form a continuous layer completely covered the electrode surface. The surface coverage of the nanoparticles on the graphite electrode surface increased as the number of ALD reaction cycles increased from 200 to 400. To determine the chemical composition of the TiO_2-deposited surface, the as-prepared electrodes were further characterized by XPS. Fig. 2(a) shows the XPS survey of the TiO_2-deposited graphite electrode. The presence of the peaks from the Ti 2p and O 1s orbitals clearly indicate that TiO_2 was successfully deposited onto the surface of the electrode. The Ti 2p core-level spectrum exhibited a double feature at 458.2 (Ti $2p_{3/2}$) and 463.9 eV (Ti $2p_{1/2}$), and a single peak was observed in the O 1s (529.6 eV) spectrum, which is in good agreement with the values for the lattice titanium and oxygen of TiO_2, respectively, as shown in Fig. 2(a) and (b) [33]. The O 1s core-level spectrum could be deconvoluted into two peaks assigned to Ti–O (529.6 eV) and O–H (531.4 eV), evaluated by a Gaussian distribution and integrated background subtraction. When the ALD of TiO_2 was conducted using $TiCl_4$ and H_2O as reactants, the process mechanism was considered to occur via the following reaction [34]

$$TiCl_4 + 2H_2O \rightarrow TiO_2 + 4HCl \quad (1)$$

and two half-reactions can be written as:

Table 1
The discharge (lithium de-intercalation) capacity value of the lithium-ion cells containing the three different electrodes at various current rates.

Current rate	Discharge (de-intercalation) capacity (mA h g^{-1})		
	Pristine graphite	TiO_2-deposited (200 ALD cycles)	TiO_2-deposited (400 ALD cycles)
0.05 C	318	316	315
0.2 C	214	219	224
1 C	121	142	145
2 C	56	74	76
4 C	15	28	32
6 C	5	12	15

$$TiOH^* + TiCl_4 \rightarrow TiOTiCl_3^* \rightarrow HCl \quad (A)$$

$$TiCl^* + H_2O \rightarrow TiOH^* + HCl \quad (B)$$

In the process where $TiCl_4$ and H_2O are used as the precursors to grow TiO_2, the growth rate in our study was about 0.08–0.1 nm per cycle [35]. Accordingly, the signal of the O–H bonds may result from the incomplete ALD reactions and residual H_2O that has not been fully purged during the ALD process. Since the reaction at room temperature may result in physical adsorption, the typical growth rates have formerly ranged from 0.04 to 0.07 nm per cycle at substrate temperature of 100–400 °C via identical mechanism [34,36].

3.2. Electrochemical properties of the TiO_2-deposited graphite electrode

After the characterization of the structure and chemical composition, TiO_2-deposited electrode-based cells were fabricated

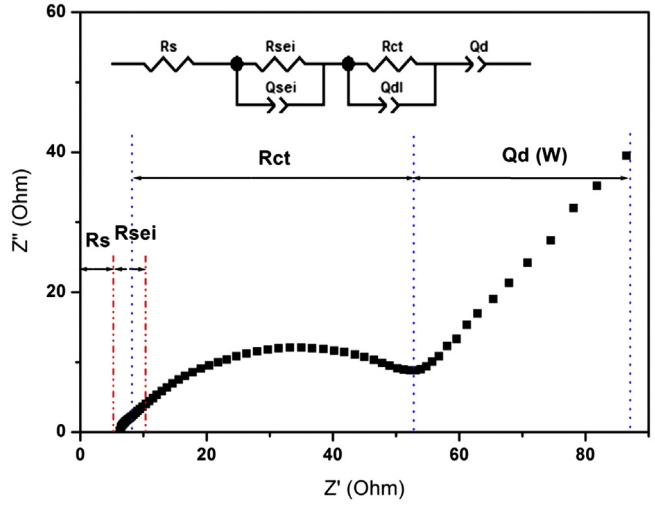

Fig. 6. The electrochemical impedance spectroscopy measurement and the equivalent circuit of the graphite negative electrode (anode). R_s, R_{sei}, R_{ct} correspond to the resistance of the ionic electrolyte, the resistance of Li^+ migration through the SEI layer and the charge-transfer resistance, respectively. Q refers to a constant phase element (CPE).

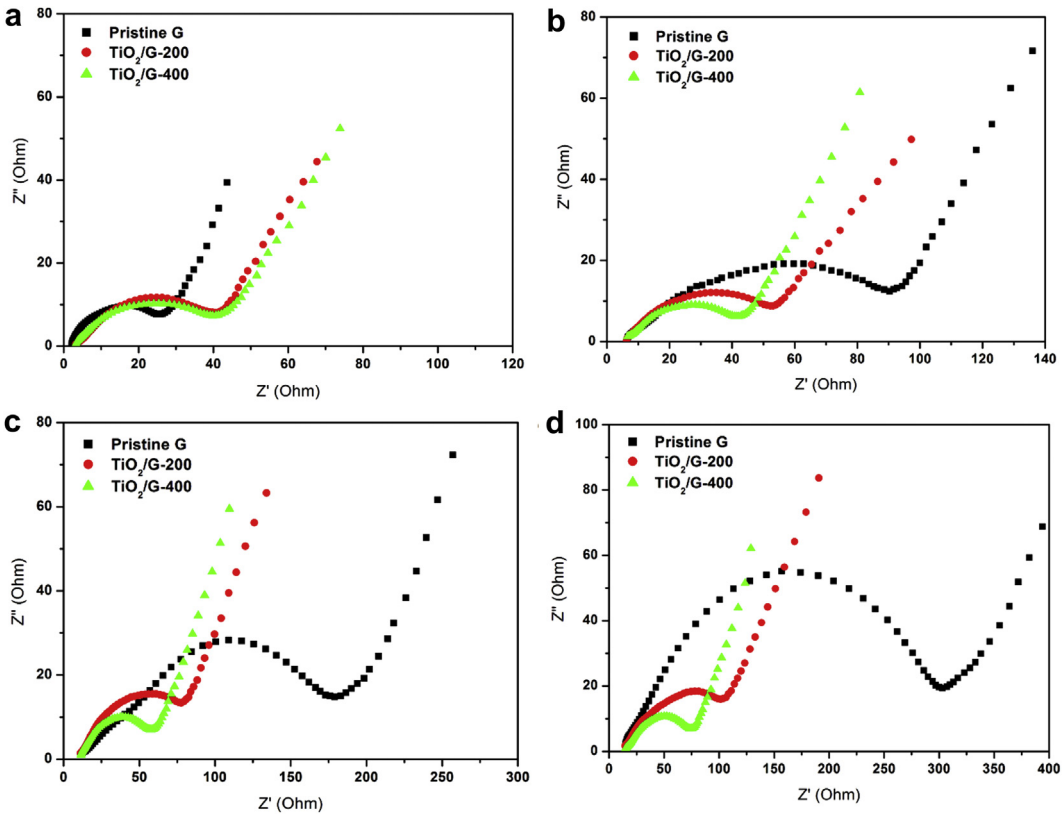

Fig. 7. Nyquist plots of the graphite electrodes and the TiO_2-deposited graphite electrode at (a) the 1st, (b) the 40th, (c) the 70th, and (d) the 100th cycles of 0.2–0.5 C charge (lithium intercalation)–discharge (de-intercalation) cycling test.

to investigate the electrochemical properties of the electrodes. Fig. 3 displays the charge (lithium intercalation)–discharge (lithium de-intercalation) curves of the pure graphite and TiO_2-deposited graphite electrode at various C-rates. At the rate of 0.05 C, the charge capacity of graphite electrode was 359 mA h g^{-1}, compared with the theoretical capacity of 372 mA h g^{-1} for the graphite. The capacity decreased rapidly with the C-rate and was almost zero at the rate of 6 C. In contrast, the charge capacity of TiO_2-deposited graphite electrode obtained after 200 and 400 ALD reaction cycles at 0.05 C were both 356 mA h g^{-1}. In other words, the surface deposition process did not change the electrochemical property of the electrode. The graphite electrodes with and without TiO_2 deposition had similar capacities at low C-rates (<0.2 C). As the C-rate increased, the advantage of surface deposition became prominent. The capacity of 200 ALD cycles TiO_2-deposited electrode was 144 mA h g^{-1}, 75 mA h g^{-1} and 29 mA h g^{-1} at 1-, 2- and 4-C rates, respectively. Specifically, the capacity of electrode with 400 ALD reaction cycles of TiO_2 deposition was 147 mA h g^{-1}, 77 mA h g^{-1} and 33 mA h g^{-1} at 1-, 2- and 4-C rates. The corresponding values for the pure graphite electrode were 122 mA h g^{-1}, 54 mA h g^{-1} and 20 mA h g^{-1}, as shown in Fig. 4. The exact discharge (de-intercalation) capacities of the electrodes are listed in Table 1. Fig. 5 shows the plot of charge (lithium intercalation) capacity as a function of the cycle number for the pure graphite and the electrodes with 200 and 400 ALD reaction cycles of TiO_2 deposition under 0.2 C lithium intercalation rate and 0.5 C de-intercalation rate. The cycle life performance of 200 ALD cycle TiO_2-deposited electrodes shows only a little better than the pristine one. But the electrodes with the 400 ALD cycle TiO_2 deposition exhibit outstanding cycle ability, compared with the general graphite electrode. We believe that the better rate capability and cycle life of the TiO_2-deposited graphite electrode are due to the nano-sized TiO_2 deposition obtained by ALD.

The electrochemical impedance spectroscopy (EIS) of the graphite electrode half cells with and without TiO_2 deposition was measured in the first, the 40th, the 70th, and the 100th cycle. A typical equivalent circuit used to fit the EIS curve is shown in Fig. 6. The resistance measured at very high frequencies corresponds to the resistance of the ionic electrolyte R_s and is added in series to the circuit. The resistance (R_{sei}) and capacitance of the solid electrolyte

Table 2
Impedance evolution of the lithium ion cells with different cycle numbers.

Cycle	Pristine graphite electrode, resistance (Ω)				TiO_2-deposited electrode (200 ALD cycles), resistance (Ω)				TiO_2-deposited electrode (400 ALD cycles), resistance (Ω)			
	R_s	R_{sei}	R_{ct}	R_{cell}	R_s	R_{sei}	R_{ct}	R_{cell}	R_s	R_{sei}	R_{ct}	R_{cell}
1	2.1	2.6	21.8	26.5	2.6	3.1	34.9	40.6	2.7	3.3	34.6	40.6
40	6.6	9.7	81.0	97.3	6.0	5.9	40.3	52.2	6.1	6.1	35.4	47.6
70	10.7	22.8	153.6	197.3	10.1	12.3	50.8	73.2	10.5	9.6	37.2	57.2
100	14.0	30.6	250.1	294.7	13.5	15.1	75.8	104.4	13.8	13.0	42.8	69.6

interphase (SEI) layer in the high frequency semicircle are related to Li^+ migration through the SEI layer. The capacitance of SEI film is represented by a constant phase element (CPE) Q_{sei}. The medium frequency semicircle is related to the charge-transfer resistance (R_{ct}) and capacitance of the double layer (Q_{dl}) on the particle surface. And a CPE (Q_d) at the low frequency region is chosen to represent the bulk diffusion of lithium ions. This approach has been used to characterize the graphite and some other active electrode materials in series and yielded a good agreement with the experimental data [37,38]. The expression for the admittance response of the CPE (Q) is

$$1/Q = C\omega^n \cos(n\pi/2) + j\omega^n \sin(n\pi/2) \quad (2)$$

where ω is the angular frequency and j is the imaginary unit. A CPE represents a resistor when $n = 0$, a capacitor with capacitance C while $n = 1$, an inductor when $n = -1$, and a Warburg resistance while $n = 0.5$.

Fig. 7 summarizes the Nyquist plots of the cells in the discharged state (0.7 V) in the first, the 40th, the 70th and the 100th cycle of the charging–discharging processes. The corresponding impedance values of lithium-ion cells with the graphite and the TiO_2 deposited electrodes in the first, the 40th, the 70th and the 100th cycles are listed in Table 2 and shown as plots in Fig. 8. In the first cycle, the R_s, R_{ct} and the total resistance R_{cell} of graphite cell are lower than those of the TiO_2-deposited graphite cells. This might be due to the low conductivity of the TiO_2. The resistance of the graphite cell increased rapidly with the cycle number while those of the TiO_2-deposited graphite cells increased rather slightly. For instance, in the 40th cycle, the 70th, and the 100th, the R_{cell} of the graphite cell increased to 97.3 Ω, 197.3 Ω, and 294.7 Ω, respectively. In contrast, the R_{cell} of the cell with 200 ALD reaction cycles TiO_2 deposition on the electrode increased to 104.4 Ω at the 100th cycle. The R_{cell} of the cell with 400 ALD reaction cycles TiO_2 deposition on the graphite electrode shows almost no change at the 40th cycle comparing to the first cycle, and it only increased to 69.6 Ω at the 100th cycle. We believe that the better cycle life capability of the TiO_2-deposited graphite cell is due to the lower cell resistance.

It is known that the total resistance (R_{cell}) of the lithium-ion cell is mainly composed of the bulk resistance of lithium ion diffusion, solid electrolyte interface resistance (R_{sei}) and charge-transfer resistance (R_{ct}) [39]. Fig. 8(c) shows the plots of R_{ct} versus the cycle number, which are similar to those of R_{cell}. As indicated in Table 1, the charge-transfer resistance (R_{ct}) contributes most of the increase in R_{cell} of the cells during prolonged cycles compared with R_s and R_{sei}. In other words, the cell impedance increase is mainly caused by the charge-transfer resistance. The R_{ct} values of the cells with graphite electrode, 200 and 400 ALD reaction cycles TiO_2-deposited graphite electrodes are 250.1 Ω, 75.8 Ω, and 42.8 Ω after 100 cycles, respectively, confirming that the lowest charge-transfer resistance is observed in the case of the cell with 400 ALD reaction cycles TiO_2-deposited graphite electrode. Therefore, our EIS results suggest that a nano scale TiO_2 deposition by ALD process on the surface of graphite electrode significantly suppressed the increase in the charge-transfer resistance during prolonged charging–discharging cycles and thus improved the electrochemical performance of the cell. The graphite or carbon anode reacts with a normal electrolyte to form the SEI passivating film which generally leads to capacity loss decreasing electronic conductivity at about 0.9 V [37]. It might be presumed that the nano-sized TiO_2 layer deposited by ALD acts as a stable inert film on the interface of electrolyte and graphite surface due to its high redox potential (i.e.

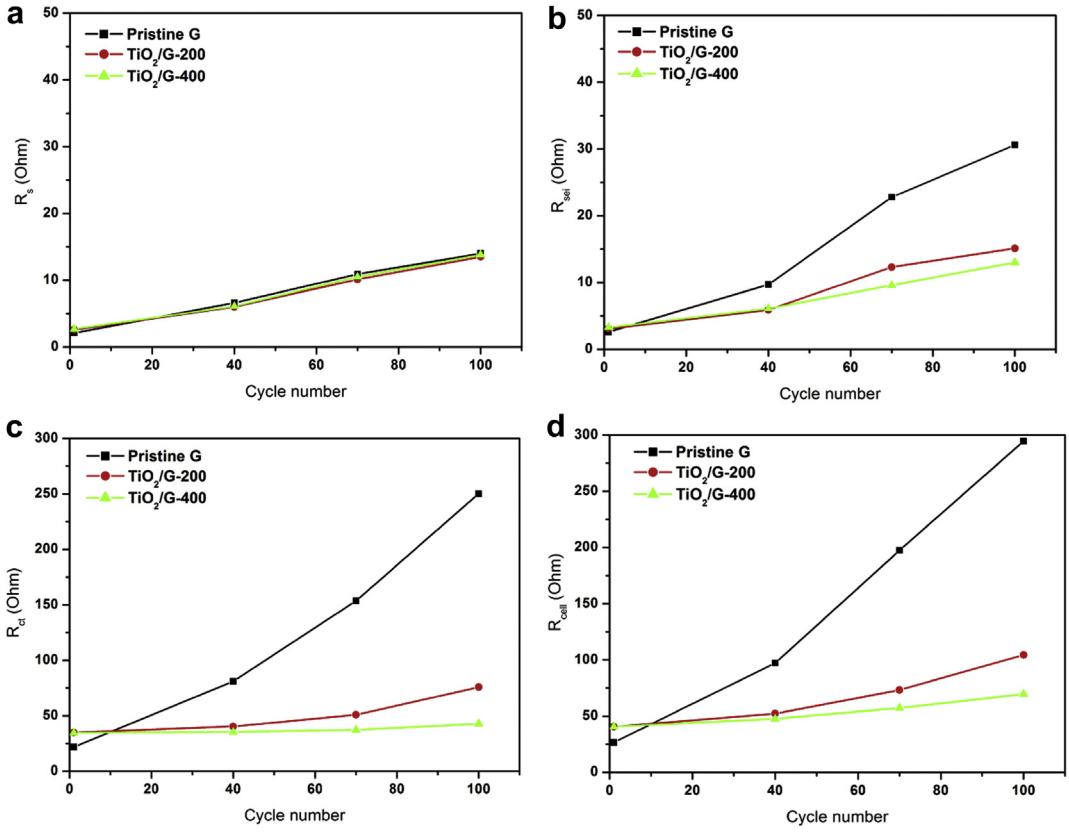

Fig. 8. Plots of (a) R_s, (b) R_{sei} (b), (c) R_{ct}, and (d) R_{cell} of the lithium-ion cells with different negative electrodes as a function of the cycle number. The cycling test condition of the cell is 0.2 C charging (lithium intercalation) and 0.5 C discharging (de-intercalation).

~1.5 V), which minimized the formation of SEI between the electrolyte and the pristine graphite electrode, thereby restraining the R_{ct} increase during the battery cycle. The superior cycle-life performances of the cell are in good agreement with the impedance spectroscopy (IS) tests.

4. Conclusion

In summary, TiO_2-deposited electrode has been successfully prepared by an ALD process. An ultra-thin nano-sized TiO_2 layer (i.e. 32–40 nm for 400 ALD cycle) was uniformly coated over the surface of the pristine graphite electrode to form a novel negative electrode for lithium ion cells. The TiO_2-deposited graphite electrode exhibited better rate-capability and cycle ability than the electrode without TiO_2 deposition. The enhanced performance is attributed to the TiO_2 deposition suppressing the increase in the charge-transfer resistance during prolonged charging–discharging cycles.

Acknowledgment

The authors would like to thank the National Science Council of the Republic of China, Taiwan, for financially supporting this research under the contract NSC 100-2622-E-034-001-CC2.

References

[1] M. Winter, J.O. Besenhard, M.E. Spahr, P. Novak, Adv. Mater. 10 (1998) 725–763.
[2] J. Shim, K.A. Striebel, J. Power Sources 119–121 (2003) 955–958.
[3] D. Aurbach, E. Zinigrad, Y. Cohen, H. Teller, Solid State Ionics 148 (2002) 405–416.
[4] J.S. Kim, Y.T. Park, J. Power Sources 91 (2000) 172–176.
[5] S.K. Jeong, M. Inaba, T. Abe, Z. Ogumi, J. Electrochem. Soc. 148 (2001) A989–A993.
[6] P. Verma, P. Mairw, P. Novak, Electrochim. Acta 55 (2010) 6332–6341.
[7] J.O. Besenhard, M. Winter, J. Yang, W. Biberacher, J. Power Sources 54 (1995) 228–231.
[8] D. Aurbach, M.D. Levi, A. Schechter, J. Phys. Chem. B 101 (1997) 2195–2206.
[9] J. Vetter, P. Novak, M.R. Wagner, C. Veit, K.C. Moller, J.O. Besenhard, M. Winter, M. Wohlfahrt-Mehrens, C. Vogler, A. Hammouche, J. Power Sources 147 (2005) 269–283.
[10] Y.P. Wu, C. Jiang, C. Wang, R. Holze, Solid State Ionics 156 (2003) 283–290.
[11] Y.P. Wu, E. Rahm, R. Holze, J. Power Sources 114 (2003) 228–236.
[12] J.J. Li, X.M. He, C.Y. Jiang, C.R. Wan, J. New Mater. Electrochem. Syst. 9 (2006) 21–23.
[13] M. Yoshio, H. Wang, K. Fukuda, Y. Hara, Y. Adachi, J. Electrochem. Soc. 147 (2000) 1245–1250.
[14] J.P. Olivier, M. Winter, J. Power Sources 151–155 (2001) 151–155.
[15] T. Placke, V. Siozios, R. Schmitz, S.F. Lux, P. Bieker, C. Colle, H.W. Meyer, S. Passerini, M. Winter, J. Power Sources 200 (2012) 83–91.
[16] P. Novák, J.C. Panitz, F. Joho, M. Lanz, R. Imhof, M. Coluccia, J. Power Sources 90 (2000) 52–58.
[17] M. Winter, Z. Phys. Chem. 223 (2009) 1395–1406.
[18] K.K. Guo, Q.M. Pan, S.B. Fan, J. Power Sources 111 (2002) 350–356.
[19] H. Zhao, J. Ren, X. He, J. Li, C. Jiang, C. Wang, Electrochim. Acta 52 (2007) 6006–6011.
[20] A. Sakuda, H. Kitaura, A. Hayashi, K. Tadanaga, M. Tatsumisago, J. Electrochem. Soc. 156 (2009) A27–A32.
[21] J.W. Lee, S.M. Park, H.J. Kim, J. Power Sources 188 (2009) 583–587.
[22] N. Kosova, E. Devyatkina, A. Slobodyuk, V. Kaichev, Solid State Ionics 179 (2008) 1745–1749.
[23] H.P. Zhang, L.C. Yang, L.J. Fu, Q. Cao, D.L. Sun, Y.P. Wu, R. Holze, J. Solid State Electrochem. 13 (2008) 1521–1527.
[24] M.L. Lee, Y.H. Li, S.C. Liao, J.M. Chen, J.W. Yeh, H.C. Shih, Appl. Surf. Sci. 258 (2012) 5938–5942.
[25] R.L. Puurunen, J. Appl. Phys. 97 (2005) 121301.
[26] G.D. Wilk, R.M. Wallace, J.M. Anthony, J. Appl. Phys. 89 (2001) 5243.
[27] L. Niinisto, M. Ritala, M. Leskela, Mater. Sci. Eng., B 41 (1996) 23–29.
[28] M. Ritala, M. Leskela, J.P. Dekker, C. Mutsaers, P.J. Soininen, J. Skarp, Chem. Vap. Deposition 5 (1999) 7.
[29] X. Meng, X.Q. Yang, X. Sun, Adv. Mater. 24 (2012) 3589–3615.
[30] Z. Yang, D. Choi, S. Kerisit, K.M. Rosso, D. Wang, J. Zhang, G. Graff, J. Liu, J. Power Sources 192 (2009) 588–598.
[31] Y.C. Chang, J.H. Jong, G.T.K. Fey, J. Electrochem. Soc. 147 (2000) 2033–2038.
[32] C.S. Wang, A.J. Appleby, F.E. Little, Electrochim. Acta 46 (2001) 1793–1813.
[33] J. Chastain, R.C. King (Eds.), Handbook of X-ray Photoelectron Spectroscopy, Physical Electronics, Physical Electronics, Eden Prairie, MN, 1995.
[34] J.D. Fergusona, A.R. Yoderb, A.W. Weimerb, S.M. George, Appl. Surf. Sci. 226 (2004) 393–404.
[35] C.C. Wang, C.C. Kei, T.P. Perng, Nanotechnology 22 (2011) 365702.
[36] Y.C. Liang, C.C. Wang, C.C. Kei, Y.C. Hsueh, W.H. Cho, T.P. Perng, J. Phys. Chem. C 115 (2011) 9498–9502.
[37] S. Zhang, P. Shi, Electrochim. Acta 49 (2004) 1475–1482.
[38] Q.C. Zhuang, T. Wei, L.L. Du, Y.L. Cui, L. Fang, S.G. Sun, J. Phys. Chem. C 114 (2010) 8614–8621.
[39] S.S. Zhang, K. Xu, T.R. Jow, J. Power Sources 160 (2006) 1403–1409.